Pramana – J. Phys. (2021) 95:4
https://doi.org/10.1007/s12043-020-02037-1
© Indian Academy of Sciences

Second law analysis of MHD third-grade fluid flow through the microchannel

MACHA MADHU[1], N S SHASHIKUMAR[1,*], B J GIREESHA[1] and NAIKOTI KISHAN[2]

[1]Department of Studies and Research in Mathematics, Kuvempu University, Shankaraghatta, Shimoga 577 451, India
[2]Department of Mathematics, Osmania University, Hyderabad 500 007, India
*Corresponding author. E-mail: shashinsbr@gmail.com

MS received 11 May 2020; revised 11 August 2020; accepted 8 September 2020

Abstract. The present study analyses the phenomena of entropy generation of magneto third-grade fluid flow through the microchannel. The significance of Joule heating, viscous heating and internal heat source is also scrutinised. The non-dimensional forms of the corresponding governing equations of the physical phenomenon with the associated boundary conditions for third-grade fluid flow and heat transfer has been solved using finite element method. The impact of various parameters on the flow and heat transfer behaviour, entropy generation and Bejan number is explained using graphs. The obtained results are examined through the plots. The results showed that an increase in the fluid parameter reduces the activity of the fluid flow and, as a result, the temperature is diminished. An enhancement in fluid motion and temperature is obtained by increasing the viscosity index. We noted that the effect of Hartmann number on the rate of local entropy generation and Bejan number is sinusoidal in nature.

Keywords. Third-grade fluid; microchannel; entropy generation; Bejan number; Reynold's model.

PACS Nos **44.15.+a; 44.20.+b; 44.40.+a**

1. Introduction

Microchannel flow is important in numerous real-life areas like microelectronics, microchips in computers, cooling of electronic devices, micromixers, microturbines, fuel cells, microelectronics, magnetohydrodynamics (MHD), micropumps etc. In this context, some important applications of fluid flow in microchannel are reported in refs [1–17]. Malvandi and Ganji [5] theoretically investigated the impact of heat transfer by convection and magnetic field on alumina/water nanofluid flow in a circular microchannel. Hedayati and Domairry [6] scrutinised the linear slip effect on mixed convective nanofluid flow through a vertical microchannel with asymmetric heating. Thermal characteristics of magnetic field on steady mixed convection flow through a porous vertical microchannel were analysed by Jha and Aina [7]. Karimipour *et al* [9] scrutinised the impact of forced convection of nanofluid flow across a microchannel. Recently, micropolar nanofluid flow through an inclined microchannel was numerically investigated by Shashikumar *et al* [17] in the presence of convective boundary conditions. This study may provide useful information to improve the thermal management of microelectromechanical systems.

Entropy generation analysis has wide applications in practical and real-life situations such as solar power collectors, heat engines, heat pumps, refrigerators etc. Entropy production additionally portrays the performance of thermal machines such as power plants, air conditioners, heat pumps, refrigerators and heat engines. The entropy generation minimisation in a thermal system was first developed by Bejan [18]. Ibánez and Cuevas [19] investigated the dissipative process that arose in a microchannel flow subjected to electromagnetic interactions. Jana and Das [20] examined the second law analysis in a flow of electrically conducting viscous fluid between horizontal plates with Navier slip effect. Ibánez [21] analysed the effects of magnetic field, hydrodynamic slip, convective boundary condition and suction/injection on entropy generation of an MHD fluid through a microchannel. Rashed [22] numerically studied the entropy generation of heat transfer and unsteady fluid flow in a porous medium with effect of magnetic and chemical reaction. Impact of forced convection flow inside a vertical microchannel has been

Published online: 03 February 2021

studied by Abbaszadeh *et al* [23]. They included the effect of slip and temperature jump in the boundary condition. Khan *et al* [24] addressed the impact of entropy production of Powell– Eyring fluid through a microchannel. Hayat *et al* [25] considered the carbon nanotubes to investigate the flow and heat transfer along with stretched nonlinear sheet. Qayyum *et al* [26] investigated the entropy generation aspects of Williamson fluid flow through two rotating disks. Javed *et al* [27] discussed the Jeffrey nanomaterial subjected to variable thickness surface in the presence of nonlinear radiative heat flux and convective heating. It is found that temperature is enhanced for increasing values of radiative heat flux and Eckert number. The same concept has been interestingly utilised by many researchers [28–31].

Studies associated with non-Newtonian third-grade fluids transmission with heat transport are an imperative research area due to their huge applications in engineering and industry. Also, the third-grade liquid models can be utilised in polymer flows. Third-grade fluid is a subcategory of non-Newtonian fluid which captures the non-Newtonian effects such as shear thinning, shear thickening as well as normal stresses, even in cases of rigid boundary. It also exhibits viscous elastic fluid characteristics. Hayat *et al* [32] have obtained the solutions by applying homotopy analysis method (HAM) to transport a third-grade fluid in a porous channel with transpiration cooling. Sajid and Hayat [33] applied HAM to analyse the parallel plate flow of third-grade fluid for constant viscosity. Effectiveness of slip conditions was explained by Ellahi *et al* [34] on nonlinear transport of third-grade fluid. Aiyesimi *et al* [35] presented the MHD flow and heat transfer in third-grade fluid through a permeable inclined plane. Baoku *et al* [36] examined the mass and heat transfer of a viscoelastic third-grade fluid over an insulated vertical plate subjected to suction across the boundary layer. Nayak *et al* [37] studied the third-grade fluid flow under the influence of radial magnetic field in wire coating process. Ogunsola and Peter [38] deliberated the impacts of Arrhenius reaction on third-grade flow with radiative heat. Rashidi *et al* [39] discussed the MHD flow of a non-Newtonian third-grade fluid over a linearly stretching sheet subjected to convective heating. Adesanya *et al* [40] analysed the convective heating of inherent irreversibility in the flow of third-grade fluid through a channel.

Motivated by the above studies, we plan to do the thermal analysis of MHD third-grade fluid flow through a porous microchannel. In the following sections, the problem is first modelled and then variational finite element method is applied to obtain numerical outcomes. The physical interpretation of the effects of embedded parameters is presented through graphs. Also, the entropy generation and Bejan number are calculated and discussed. The study presented in this paper can be used to do further studies on thin film flow, energy conservation, coal-water mixture, polymer solution and oil recovery applications. The outcomes are also useful in many geological and petrochemical engineering systems, in which energy is maximised.

2. Governing equations and physical model

Here steady MHD third-grade fluid flow caused by a parallel plate microchannel has been considered. The third-grade fluid is injected constantly into microchannel at the lower plate and third-grade fluid is sucked by the upper plate. The upper plate is placed at $y^* = h$ while the lower plate is placed at $y^* = 0$, y^* denoting the transversal coordinates. In addition, T_1 and T_2 denote the temperature of lower plate/upper plate respectively (see figure 1). Both the plates are infinitely long and so velocity fields are fully developed. Hence, physical quantities depend on the transversal y^* coordinate only. Also, magnetic field of uniform strength B_0 is applied normal to the plates. Moreover, convective boundary condition and viscous dissipation are accounted. Based on the above assumptions, the flow governing equations

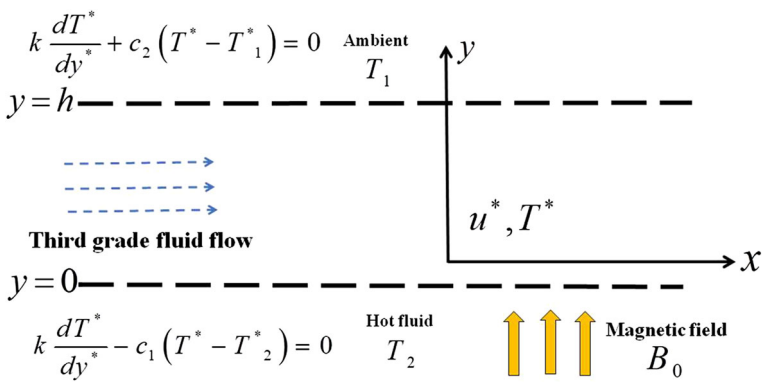

Figure 1. Geometry of the flow problem.

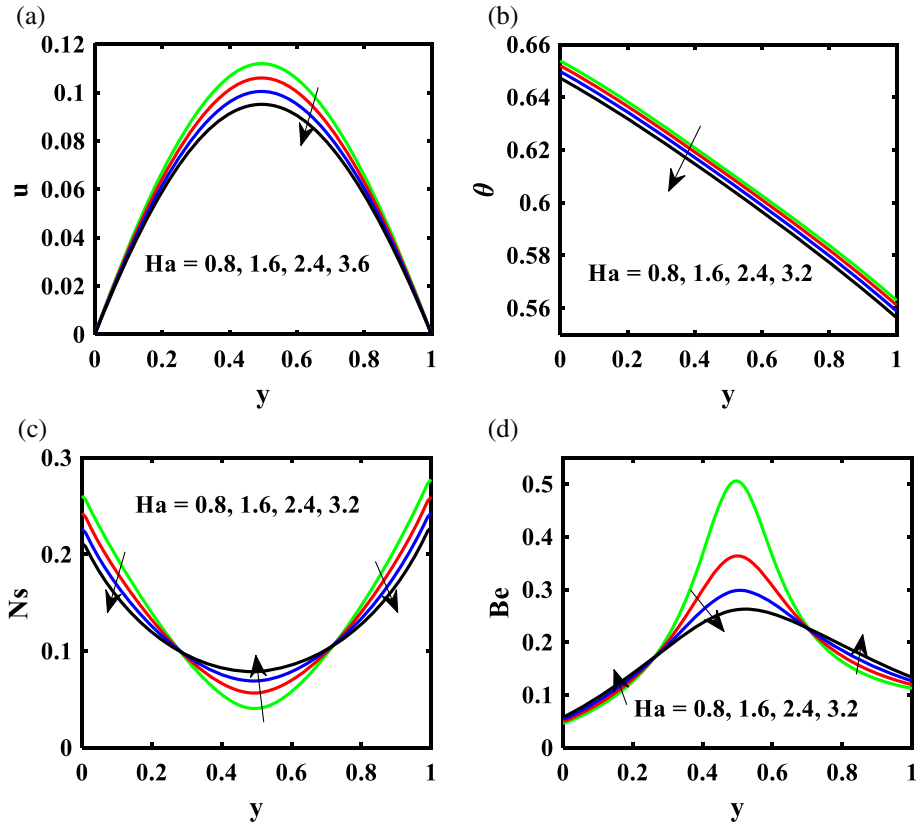

Figure 2. Effect of Ha on (**a**) velocity ($u\,(y)$), (**b**) temperature ($\theta\,(y)$), (**c**) entropy generation (Ns) and (**d**) Bejan Number (Be).

in mathematical form under respective boundary situation are written as [21,22]

$$\frac{\mathrm{d}}{\mathrm{d}y^*}\left(\mu^*\frac{\mathrm{d}u^*}{\mathrm{d}y^*}\right)+6\beta\left(\frac{\mathrm{d}u^*}{\mathrm{d}y^*}\right)\frac{\mathrm{d}^2u^*}{\mathrm{d}y^{*2}} -\frac{\phi u^*}{k_1}\left[\mu^*+2\beta\left(\frac{\mathrm{d}u^*}{\mathrm{d}y^*}\right)^2\right]-\sigma B_0^2u^*=\frac{\partial p}{\partial x}, \tag{1}$$

$$k\frac{\mathrm{d}^2T^*}{\mathrm{d}y^{*2}}+\mu^*\left(\frac{\mathrm{d}u^*}{\mathrm{d}y^*}\right)^2+2\beta\left(\frac{\mathrm{d}u^*}{\mathrm{d}y^*}\right)^4 -\frac{\partial q_r}{\partial y^*}+\sigma B_0^2u^{*2}=0, \tag{2}$$

$$u^*=0,\ k\frac{\mathrm{d}T^*}{\mathrm{d}y^*}-c_1\left(T^*-T_2\right)=0 \text{ at } y^*=0, \tag{3}$$

$$u^*=0,\ k\frac{\mathrm{d}T^*}{\mathrm{d}y^*}+c_2\left(T^*-T_1\right)=0 \text{ at } y^*=h, \tag{4}$$

where μ^* is the viscosity coefficient, u^* is the axial velocity, p is the pressure, σ is the electrical conductivity, ϕ is the porosity of porous space, T^* is the fluid temperature, β is the non-Newtonian parameter, T_1 is the ambient temperature, k_1 is the permeability, k is the thermal conductivity, T_2 is the hot fluid temperature, q_r is the radiative heat flux and c_1, c_2 are the convective heat transfer coefficients.

Radiative flux is calculated via Rosseland assumption appeared in eq. (2):

$$q_r=-\frac{16\sigma_1}{3\chi}T_1^3\frac{\mathrm{d}T^*}{\mathrm{d}y^*}, \tag{5}$$

where χ is the Rosseland mean absorption coefficient and σ_1 is the Stefan–Boltzmann constant.

Using eq. (5) in (2) we get

$$\left(k+\frac{16\sigma_1}{3\chi}T_1^3\right)\frac{\mathrm{d}^2T^*}{\mathrm{d}y^{*2}}+\mu^*\left(\frac{\mathrm{d}u^*}{\mathrm{d}y^*}\right)^2 +2\beta\left(\frac{\mathrm{d}u^*}{\mathrm{d}y^*}\right)^4+\sigma B_0^2u^{*2}=0. \tag{6}$$

The following dimensionless variables

$$u=\frac{u^*}{U},\quad y=\frac{y^*}{h},\quad \mu=\frac{\mu^*}{\mu_0},\quad \theta=\frac{T^*-T_1}{T_2-T_1}, \tag{7}$$

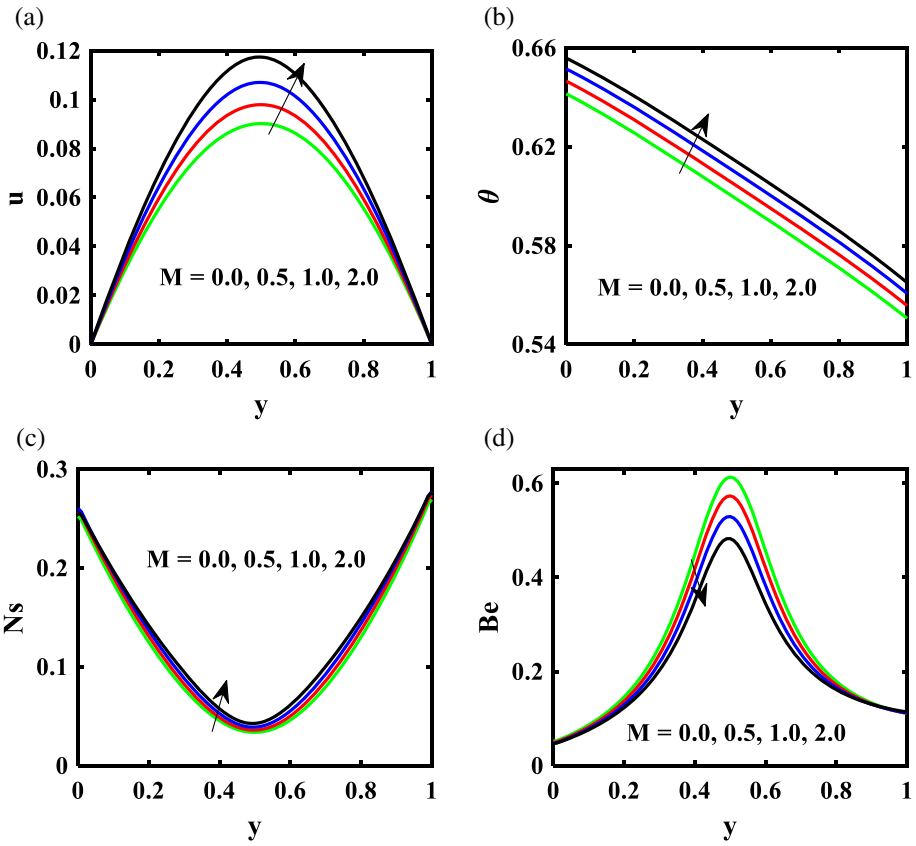

Figure 3. Effect of M on (**a**) velocity ($u\,(y)$), (**b**) temperature ($\theta\,(y)$), (**c**) entropy generation (Ns) and (**d**) Bejan Number (Be).

are substituted into eqs (1)–(4) and (6) to get

$$\frac{\mathrm{d}}{\mathrm{d}y}\left(\mu\frac{\mathrm{d}u}{\mathrm{d}y}\right)+6\lambda_1\left(\frac{\mathrm{d}u}{\mathrm{d}y}\right)^2\frac{\mathrm{d}^2u}{\mathrm{d}y^2} -\lambda_2 u\left[\mu+2\lambda_1\left(\frac{\mathrm{d}u}{\mathrm{d}y}\right)^2\right]-Hau=P, \tag{8}$$

$$(1+Rd)\,\frac{\mathrm{d}^2\theta}{\mathrm{d}y^2}+\mu\Lambda\left(\frac{\mathrm{d}u}{\mathrm{d}y}\right)^2 +\Lambda\left[2\lambda_1\left(\frac{\mathrm{d}u}{\mathrm{d}y}\right)^4+Hau^2\right]=0, \tag{9}$$

$$u=0,\ \theta'-Bi_1\,(\theta-1)=0 \text{ at } y=0, \tag{10}$$

$$u=0,\ \theta'+Bi_2\,(\theta)=0 \text{ at } y=1, \tag{11}$$

where μ_0 is the reference viscosity, u is the arbitrary reference velocity,

$$Ha=\frac{\sigma B_0^2h^2}{\mu_0}$$

is the Hartmann number,

$$\lambda_1=\frac{\beta U^2}{\mu_0h^2}$$

is the parameter related to the non-Newtonian behaviour,

$$\lambda_2=\frac{\phi h^2}{k_1}$$

is the parameter for the porosity of the media,

$$P=\frac{h^2}{\mu_0U}\frac{\partial p}{\partial x}$$

is the pressure gradient parameter,

$$Bi_{1,2}=hc_i/k \ \text{ for } i=1,2$$

is the Biot number for the upper/lower plate,

$$Rd=\frac{16\sigma_1T_1^3}{3k\chi}$$

is the radiation parameter and

$$\Lambda=\frac{\mu_0U_2^2}{k(T_2-T_1)}$$

is the viscous dissipation parameter.

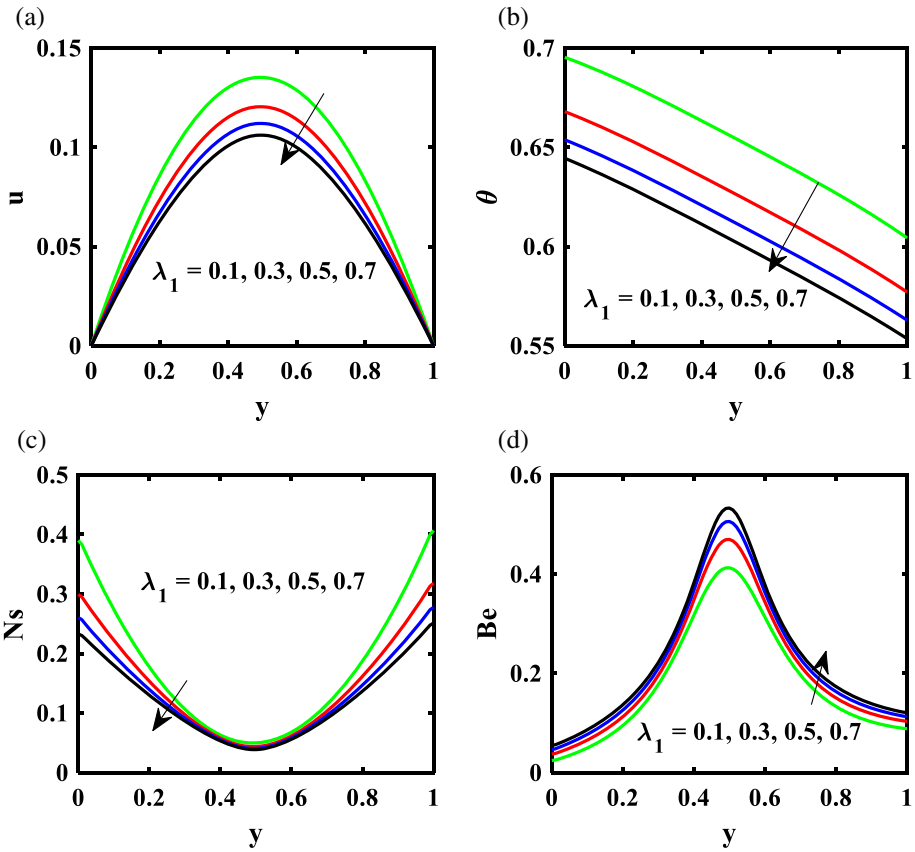

Figure 4. Effect of λ_1 on (**a**) velocity ($u\,(y)$), (**b**) temperature ($\theta\,(y)$), (**c**) entropy generation (Ns) and (**d**) Bejan Number (Be).

3. Entropy production

The entropy generation rate (E_g) for the third-grade fluid in the presence of magnetic field with heat transfer in a microchannel is given as

$$E_g = \frac{1}{T_1^2}\left(k + \frac{16\sigma_1 T_1^3}{3\chi}\right)\left(\frac{\mathrm{d}T^*}{\mathrm{d}y^*}\right)^2 + \frac{\mu^*}{T_1}\left(\frac{\mathrm{d}u^*}{\mathrm{d}y^*}\right)^2 + \frac{2\beta}{T_1}\left(\frac{\mathrm{d}u^*}{\mathrm{d}y^*}\right)^4 + \frac{1}{T_1}\sigma B_0^2 u^{*2}. \tag{12}$$

The dimensionless expression for entropy generation is given as

$$Ns = \frac{E_g}{E_{g0}} = (1+Rd)\left(\frac{\mathrm{d}\theta}{\mathrm{d}y}\right)^2 + \mu\Lambda\left(\frac{\mathrm{d}u}{\mathrm{d}y}\right)^2 + \frac{\Lambda}{\mathrm{L}}\left[2\lambda_1\left(\frac{\mathrm{d}u}{\mathrm{d}y}\right)^4 + Hau^2\right]. \tag{13}$$

$$Ns = N_h + N_v. \tag{14}$$

In eqs (13) and (14)

$$E_{g0} = \frac{k\,(T_2 - T_1)^2}{h^2 T_1^2}$$

is the characteristic entropy generation rate,

$$L = \frac{T_2 - T_1}{T_1}$$

is the characteristic temperature ratio,

$$N_h = (1+Rd)\left(\frac{\mathrm{d}\theta}{\mathrm{d}y}\right)^2$$

is the irreversibility heat transfer and

$$N_v = \mu\Lambda\left(\frac{\mathrm{d}u}{\mathrm{d}y}\right)^2 + \frac{\Lambda}{\mathrm{L}}\left[2\lambda_1\left(\frac{\mathrm{d}u}{\mathrm{d}y}\right)^4 + Hau^2\right]$$

is the dissipative irreversibility.

The Bejan number (Be) is defined as

$$Be = \frac{\text{Irreversibility heat transfer}}{\text{Total entropy generation } (Ns)}.$$

Numerically we have

$$Be = \frac{N_h}{N_h + N_v} = \frac{N_h}{N_s}. \tag{15}$$

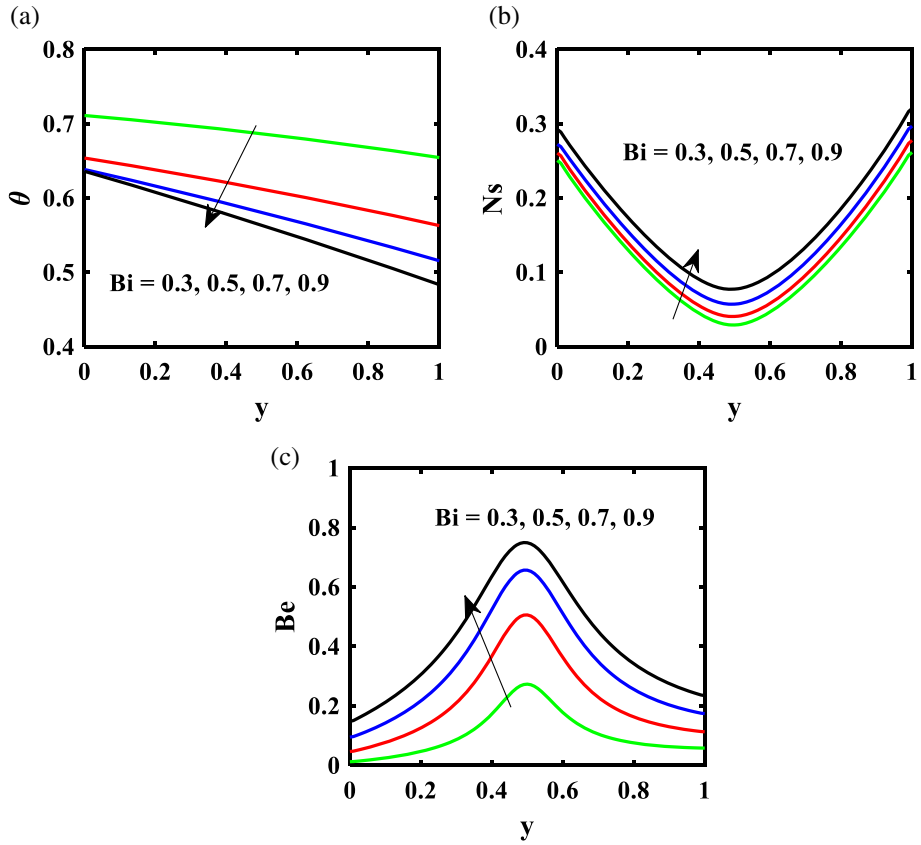

Figure 5. Effect of Bi on (**a**) temperature ($\theta\,(y)$), (**b**) entropy generation (Ns) and (**c**) Bejan Number (Be).

4. Reynold's Model

In this paper, Reynold's model is used to account for the variation of viscosity with temperature. The viscosity (μ) for Reynold's model is expressed as

$$\mu = \mathrm{e}^{-M\theta}. \tag{16}$$

By using Taylor series expansion, we get

$$\mu = 1 - M\theta, \quad \frac{\mathrm{d}\mu}{\mathrm{d}y} = -M\frac{\mathrm{d}\theta}{\mathrm{d}y}, \tag{17}$$

where M is the viscosity index.

Substituting eq. (17) into eqs (8), (9) and (13) gives

$$(1 - M\theta)\frac{\mathrm{d}^2u}{\mathrm{d}y^2} - M\frac{\mathrm{d}\theta}{\mathrm{d}y}\frac{\mathrm{d}u}{\mathrm{d}y} + 6\lambda_1\left(\frac{\mathrm{d}u}{\mathrm{d}y}\right)^2\frac{\mathrm{d}^2u}{\mathrm{d}y^2} - \lambda_2 u\left[(1-M\theta)+2\lambda_1\left(\frac{\mathrm{d}u}{\mathrm{d}y}\right)^2\right] - Hau = P, \tag{18}$$

$$(1 + Rd)\frac{\mathrm{d}^2\theta}{\mathrm{d}y^2} + (1 - M\theta)\,\Lambda\left(\frac{\mathrm{d}u}{\mathrm{d}y}\right)^2 + \Lambda\left[2\lambda_1\left(\frac{\mathrm{d}u}{\mathrm{d}y}\right)^4 + Hau^2\right] = 0, \tag{19}$$

$$Ns = \frac{E_g}{E_{g_0}} = (1 + Rd)\left(\frac{\mathrm{d}\theta}{\mathrm{d}y}\right)^2 + (1-M\theta)\Lambda\left(\frac{\mathrm{d}u}{\mathrm{d}y}\right)^2 + \frac{\Lambda}{\mathrm{L}}\left[2\lambda_1\left(\frac{\mathrm{d}u}{\mathrm{d}y}\right)^4 + Hau^2\right]. \tag{20}$$

5. Results and discussion

Suitable transformation is used to transform the nonlinear differential equations (8) and (9) into dimensionless ordinary differential equations (ODEs), which can be solved by using finite element method. For the entire numerical computation, dimensionless parameters are taken $\lambda_1 = 0.5$, $\lambda_2 = 1.2$, $M = 0.5$, $P = -1$, $Rd = 1.5$, $\Lambda = 2$, $Bi = 0.5$, $Ha = 0.8$. The effect of various parameters on the flow and heat transfer phenomenon is explained through graphs.

5.1 *Effect of Hartmann Number (Ha) on various profiles*

Impact of Hartmann number (Ha) is sketched in figure 2. Generally, the geometries of velocity profile are parabolic in nature with zero values at the wall with no

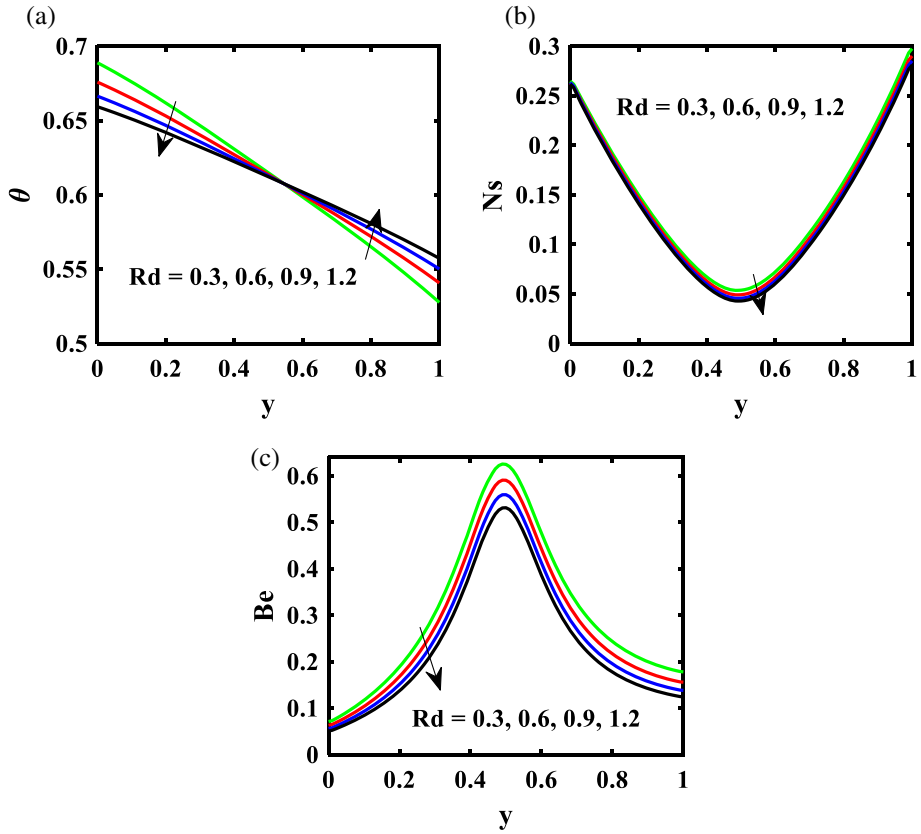

Figure 6. Effect of Rd on (**a**) temperature ($\theta\,(y)$), (**b**) entropy generation (Ns) and (**c**) Bejan Number (Be).

slip condition and maximum values within the channel. It can be noted that the velocity profile shows a declining nature to the increasing values of *Ha*. As Hartmann number is associated with Lorentz force, larger values of *Ha* produces more resistance to the flow and consequently u reduces. Now, temperature also exhibits a similar behavior as that of the velocity. As *Ha* increases, Lorentz force increases which is a favourable factor for temperature. But, due to the convective heat loss, the temperature profile exhibits an opposite behaviour. Entropy generation profile shows decreasing nature at the walls of the channel and increasing nature within the walls for increasing values of *Ha*. As *Ha* increases Bejan number (*Be*) profile shows an enhancing behaviour at the walls and a decreasing nature within the walls. When *Ha* increases at the walls, the resulting Lorentz force creates a higher pressure drop at the walls leading to an increase in *Be*. For the fluid within the walls, the increasing Lorentz force results in a lesser pressure drop which consequently results in altered nature of *Be*.

5.2 *Effects of viscosity index (M) on various profiles*

Figure 3 represents the effect of viscosity index (M) on velocity $u(y)$, temperature $\theta(y)$, entropy generation Ns and Bejan number Be. It can be noticed that the velocity profile enhances with increasing M since higher M results in a low viscosity which is favourable for the velocity. $\theta(y)$ can be seen enhancing with higher values of M. As the value of M increases, the viscosity decreases which results in an increasing internal resistance between the fluid molecules. This resistance leads to higher temperature. As M increases, viscosity decreases which results in the increased velocity and hence there is an unavailability of energy resulting in an increase in the entropy generation. Be profile shows a declining nature to the changes of M. As M increases, the viscosity decreases which results in a lower pressure drop of the fluid and a deterioration in the Be profile.

5.3 *Effect of non-Newtonian behaviour* (λ_1) *on different profiles*

Figure 4 represents the change in the profile of velocity, temperature, entropy generation Ns and Be with larger estimations of dimensionless parameter related to the non-Newtonian behaviour. As λ_1 increases, the velocity profile shows a declining nature. As λ_1 increases, the viscosity of the fluid enhances which causes a

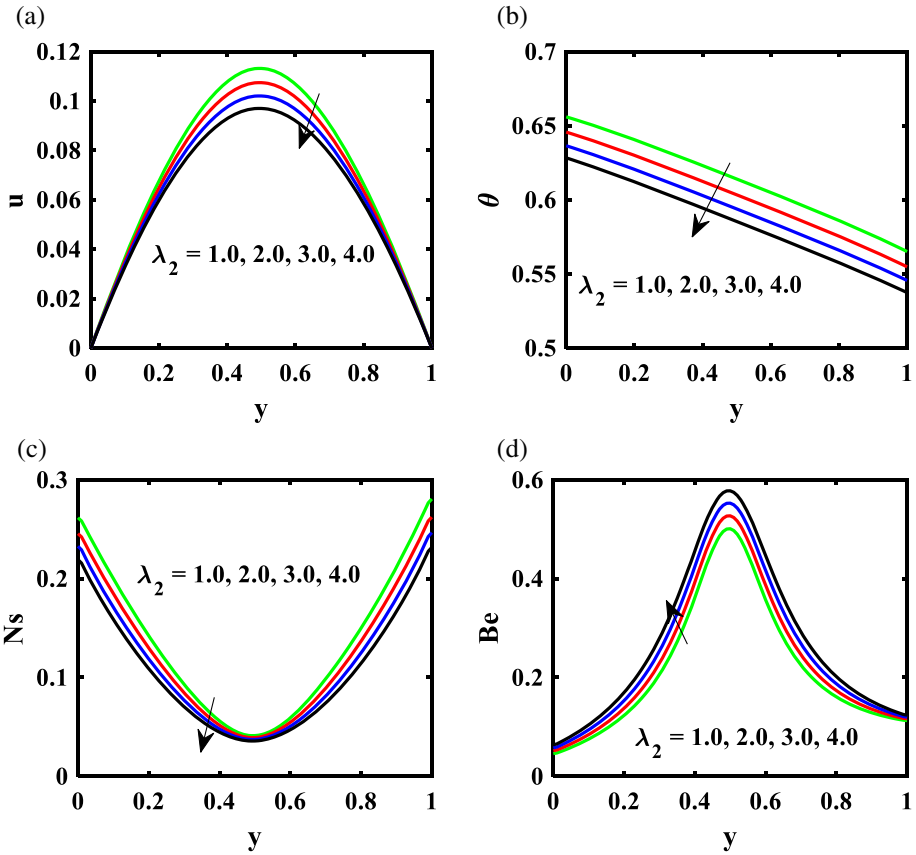

Figure 7. Effect of λ_2 on (**a**) ($u\,(y)$), (**b**) temperature ($\theta\,(y)$), (**c**) entropy generation (Ns) and (**d**) Bejan Number (Be).

decrease in velocity profile. It can be noticed that influence of λ_1 via temperature profile shows a behaviour similar to the velocity profile. Reducing impact is observed for temperature profile. It can be noted from the figure that increase in λ_1 produces more disturbance in the flow system and thus entropy generation rate becomes less, but reverse trend is observed for Be. This is because campared to irreversibility due to fluid friction, the heat transfer irreversibility is higher.

5.4 *Effect of Biot Number* (Bi) *on different profiles*

Figure 5 shows the influence of Bi on $\theta\,(y)$, Ns and Be profiles. The temperature profile clearly depicts that as Bi increases the temperature decreases due to the enhancement in internal conductive resistance which results in the decrease of temperature. It can be noted that Ns profiles show similar behaviour for raising values of Bi. Increasing Bi leads to internal conductive resistance and increase in the pressure drop. Due to this, Ns and Be profiles increase. So, we can say that the convective thermal boundary conditions increase the dominant effects of heat transfer irreversibility on the fluid flow system.

5.5 *Effect of radiation parameter* (Rd) *on different profiles*

Figure 6 depicts the effect of radiation parameter on temperature $\theta(y)$, Ns and Be profiles. Temperature profile decreases at one end of the wall and increases on the other but converges in the middle as Rd goes higher. The Ns and Be distributions show a deteriorating nature as Rd increases.

5.6 *Effect of porosity* (λ_2) *on different profiles*

Figure 7 depicts the variation in $u\,(y)$, $\theta\,(y)$, Ns and Be profiles for increasing values of dimensionless parameter of porosity. It is noticed that increasing values of $u(y)$ and $\theta(y)$ profiles show a decreasing nature to the enhancing values of λ_2. Resistance between the molecules of the fluid increases which leads to decrease in velocity and temperature. Entropy generation profile decreases as porosity increases.

5.7 *Effect of viscous dissipation on different profiles*

Figure 8 depicts the changes in the profiles of $u\,(y)$, $\theta\,(y)$, Ns and Be with increasing values of viscous

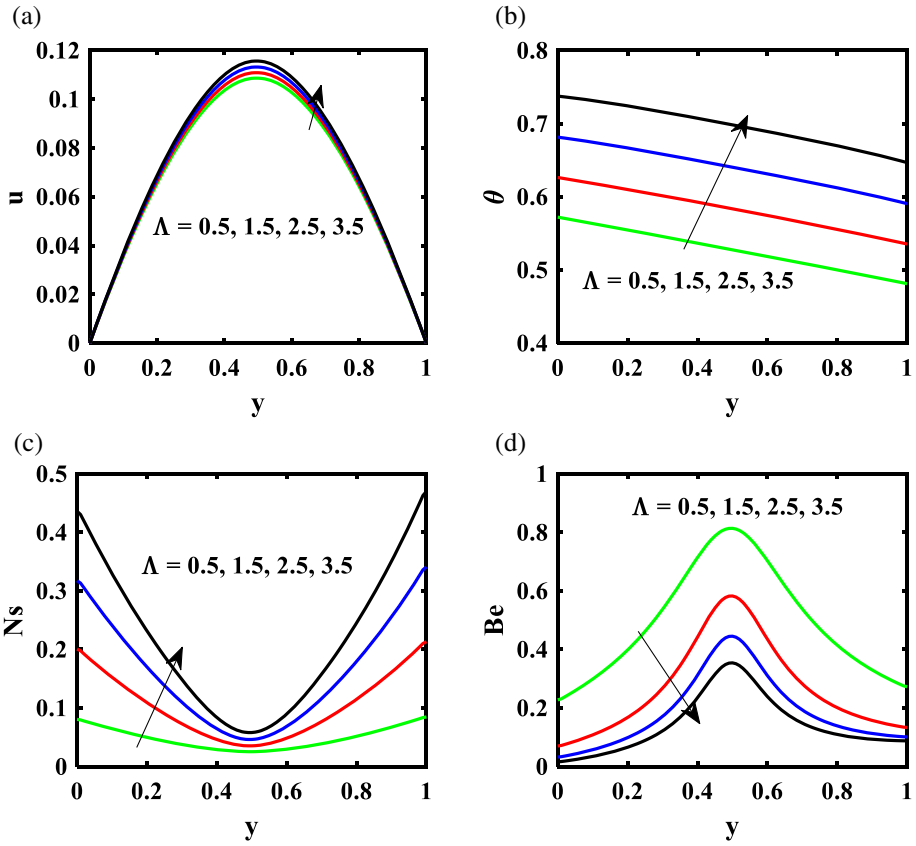

Figure 8. Effect of Λ on (**a**) velocity ($u\,(y)$), (**b**) temperature ($\theta\,(y)$), (**c**) entropy generation (Ns) and (**d**) Bejan Number (Be).

dissipation. The velocity profile increases with higher Λ values. From the figure it is found that $\theta\,(y)$ and Ns profiles are increasing with increasing Λ, but Bejan number shows opposite behaviour to the increasing values of Λ. With increasing Λ, viscosity of the fluid rises by transforming energy from the motion of the fluid and converting into internal energy leading to rise in temperature profile. Therefore, there is an inaccessibility in the transformation of thermal energy to mechanical energy as it is transformed to the internal energy. Consequently, entropy generation profile increases.

6. Conclusion

Entropy generation and heat transfer analysis of MHD flow of an incompressible third-grade fluid through a microchannel porous wall have been analysed. The problem is tackled numerically by using FEM. Based on the above presented results, the conclusions drawn are:

- Velocity profile increases on increasing M and Λ whereas it decreases on increasing Ha, λ_1 and λ_2.
- Temperature profile escalates with higher values of M and Λ while it declines for Ha, Bi, λ_1 and λ_2. In case of Rd, the temperature profile enhances at walls and declines within the walls.
- Entropy generation increases at increasing values of M, Bi and Λ whereas it deteriorates on growing values of λ_1, Rd and λ_2. At the walls, the profile increases with higher Ha and declines with lower Ha.
- Bejan number increases with escalating values of λ_1, Bi and λ_2 while it minimises for M, Rd and Λ. The Bejan number profile exhibits enhancing behaviour at the walls and decreasing nature within the walls for Ha.

Acknowledgements

One of the authors (Macha Madhu) acknowledges the UGC for financial support under the Dr. D.S. Kothari Postdoctoral Fellowship Scheme (No. F.4-2/2006 (BSR)/MA/16-17/0043). The authors extend their sincere thanks to the editor and referees of the

journal, for their valuable suggestions to improve this article.

References

[1] G M Mala, D Li and J D Dale. *Int. J. Heat Mass Transf.* **40**(**13**), 3079 (1997)
[2] C K Chen and H C Weng, *J. Heat Transfer* **127**(**9**), 1053 (2005)
[3] L B Erbay, M M Yalçın and M Ş Ercan, *Heat Mass Transfer* **43**(**8**), 729 (2007)
[4] M Sheikholeslami, M Gorji-Bandpy, D D Ganji and S Soleimani, *Adv. Powder Technol.* **24**(**6**), 980 (2013)
[5] A Malvandi and D D Ganji, *Int. J. Therm. Sci.* **84**, 196 (2014)
[6] F Hedayati and G Domairry, *Powder Technol.* **272**, 250 (2015)
[7] B K Jha and B Aina, *Ain Shams Eng. J.* **9**, 747 (2016)
[8] N S Shashikumar, B J Gireesha, B Mahanthesh, B C Prasannakumara and A J Chamkha, *Int. J. Numer. Meth. Heat Fluid Flow*, https://doi.org/10.1108/HFF-06-2018-0301 (2018)
[9] A Karimipour, A D'Orazio and M S Shadloo, *Physica E* **86**, 146 (2017)
[10] N S Shashikumar, B C Prasannakumara, B J Gireesha and O D Makinde, Thermodynamics analysis of MHD Casson fluid slip flow in a porous microchannel with thermal radiation. in: *Diffusion foundations* (Trans Tech Publications, 2018) Vol. 16, pp. 120–139
[11] N S Shashikumar, B J Gireesha, B Mahanthesh and B C Prasannakumara, *Multidiscip. Model. Mater. Struct.* **14**(**4**), 769 (2018)
[12] S R Hosseini, M Sheikholeslami, M Ghasemian and D D Ganji, *Powder Technol.* **324**, 36 (2018)
[13] A Arabpour, A Karimipour and D Toghraie, *J. Therm. Anal. Calor.* **131**(**2**), 1553 (2018)
[14] N S Shashikumar, B C Prasannakumara, M Archana and B J Gireesha, *J. Nanofluids* **8**(**1**), 63 (2019)
[15] M Madhu, N S Shashikumar, B Mahanthesh, B J Gireesha and N Kishan, *Appl. Math. Mech.* **40**(**9**), 1285 (2019)
[16] M Madhu, N S Shashikumar, B J Gireesha and N Kishan, *Phys. Scr.* **94**(**12**), 125 (2019)
[17] N S Shashikumar, M Macha, B J Gireesha and N Kishan, *Multidiscip. Model. Mater. Struct.* (2020)
[18] A Bejan, Second-law analysis in heat transfer and thermal design, in: *Advances in heat transfer* (Elsevier, 1982) Vol. 15, pp. 1–58
[19] G Ibáñez and S Cuevas, *Energy* **35**(**10**), 4149 (2010)
[20] S Das and R N Jana, *Ain Shams Eng. J.* **5**(**2**), 575 (2014)
[21] G Ibáñez, *Int. J. Heat Mass Transf.* **80**, 274 (2015)
[22] G M Rashed, *J. Appl. Math.*, https://doi.org/10.1155/2016/1748312 (2016)
[23] M Abbaszadeh, A Ababaei, A A A Arani and A A Sharifabadi, *J. Braz. Soc. Mech. Sci. Eng.* **39**(**3**), 775 (2017)
[24] A A Khan, F Zaib and A Zaman, *J. Braz. Soc. Mech. Sci. Eng.* **39**(**12**), 5027 (2017)
[25] T Hayat, M I Khan, T A Khan, M I Khan, S Ahmad and A Alsaedi, *J. Mol. Liquids* **265**(**1**), 629 (2018)
[26] S Qayyum, M I Khan, T Hayat, A Alsaedi and M Tamoor, *Int. J. Heat Mass Transf.* **127**, 933 (2018)
[27] M F Javed, M Waqas, M I Khan, N B Khan, R Muhammad, M U Rehman, S W Khan and M T Hassan, *Appl. Nanosci.* **10**, 3011 (2020)
[28] M Kumar, G J Reddy and N Dalir, *Pramana – J. Phys.* **91(5)**: 60 (2018)
[29] Z Iqbal, Z Mehmood and B Ahmad, *Pramana – J. Phys.* **90(5)**: 64 (2018)
[30] T Hayat, M Kanwal, S Qayyum, M I Khan and A Alsaedi, *Pramana – J. Phys.* **93(4)**: 54 (2019)
[31] T Hayat, F Masood, S Qayyum and A Alsaedi, *Pramana – J. Phys.* **93(6)**: 96 (2019)
[32] T Hayat, R Ellahi, P D Ariel and S Asghar, *Nonlinear Dynam.* **45(1–2)**, 55 (2006)
[33] M Sajid and T Hayat, *Trans. Porous Media* **71(2)**, 173 (2008)
[34] R Ellahi, T Hayat, F M Mahomed and S Asghar, *Nonlinear Anal.: Real World Appl.* **11**(**1**), 139 (2010)
[35] Y M Aiyesimi, G T Okedayo and O W Lawal, *Math. Theory Model* **2**(**9**), https://www.iiste.org/Journals/index.php/MTM/article/view/2789 (2012)
[36] I G Baoku, B I Olajuwon and A O Mustapha, *Int. J. Heat Fluid Flow* **40**, 81 (2013)
[37] M K Nayak, G C Dash and L P Singh, *Int. J. Heat Mass Transf.* **79**, 1087 (2014)
[38] A W Ogunsola and B A Peter, *Int. J. Pure Appl. Sci. Tech.* **22**(**1**), 1 (2014)
[39] M M Rashidi, S Bagheri, E Momoniat and N Freidoonimehr, *Ain Shams Eng. J.* **8**(**1**), 77 (2017)
[40] S O Adesanya, J A Falade, S Jangili and O A Beg, *Alex. Eng. J.* **56**(**1**), 153 (2017)